DEPARTMENT OF DEFENCE
DEFENCE SCIENCE & TECHNOLOGY ORGANISATION
DSTO

DSTO

Refractivity Profile Assimilation Model for the Atmospheric Boundary Layer

D. M. Phillips and C. P. Baker

DSTO-RR-0148

Refractivity Profile Assimilation Model for the Atmospheric Boundary Layer

D. M. Phillips and C. P. Baker

Surveillance Systems Division
Electronics and Surveillance Research Laboratory

DSTO-RR-0148

ABSTRACT

Anomalous propagation of microwave radiation in the Atmospheric Boundary Layer (ABL) at near horizontal elevation angles due to small vertical gradients in the refractive index of the air can significantly enhance or degrade the performance of microwave systems. The modelling of microwave propagation under anomalous ducting conditions requires an accurate knowledge of the vertical profile of atmospheric refractivity, which can be derived from profiles of pressure, temperature and moisture. This paper develops the Monin-Obukhov similarity theory of the atmospheric surface layer by blending it into the mixed layer, which lies above it and which forms the bulk of the atmospheric boundary layer. This approach enables the optimal assimilation of meteorological data from a variety of heights in the ABL and a sensitivity analysis provides the necessary weight functions. Application of the theory to one set of data over sea shows that a significant improvement in the fit to the data is achieved when the roughness length for heat is assumed to be much greater than the roughness length for wind.

RELEASE LIMITATION

Approved for public release

DEPARTMENT OF DEFENCE
DEFENCE SCIENCE & TECHNOLOGY ORGANISATION
DSTO

Published by

DSTO Electronics and Surveillance Research Laboratory
PO Box 1500
Salisbury South Australia 5108 Australia

Telephone: (08) 8259 5555
Fax: (08) 8259 6567

AR-010-884
July 1999

APPROVED FOR PUBLIC RELEASE

Refractivity Profile Assimilation Model for the Atmospheric Boundary Layer

Executive Summary

Anomalous propagation of microwave radiation in the lower parts of the troposphere due to varying meteorological conditions can significantly enhance or degrade the performance of microwave systems, including communication, radar, ESM, weapon and decoy systems. In particular, the performance of surveillance radars on Navy ships can be significantly affected by local changes in temperature and humidity. Depending on the prevailing meteorological conditions and the placement of the antennas on the ships, maximum radar detection ranges of low-altitude targets may be either significantly enhanced or significantly degraded due to the ducting of the radiation caused by high vertical gradients of moisture or temperature.

The Surveillance Systems Division has recently delivered to Navy the Tropospheric Refractive Effects Prediction System (TREPS), which is a computer program designed to predict the performance of surveillance radars and ESM systems on board Navy ships, submarines and maritime patrol aircraft. Crucial to the accuracy of the predictions is the need for the program to have an accurate description of the refractivity profile of the atmosphere through which the radiation propagates.

In the past, it was necessary to ensure that the measurements of temperature and humidity as a function of height were made below a critical height known as the Surface Layer height, commonly between about 10 and 100 metres above sea level. Unfortunately, it is not possible to evaluate this height without *a priori* information about the profiles of temperature and humidity. This report describes the theory behind a method of determining the required meteorological information from measurements of temperature and humidity at *any* height within the first few hundred metres above sea level. The results of this research have been incorporated into the TREPS Version 2.2.1 software, thus allowing the operators of the package more freedom in supplying the required meteorological information needed to perform accurate calculations of the performance of their radars and other microwave systems.

Authors

Dr David M. Phillips
Surveillance Systems Division

Dr David Phillips is a Principal Research Scientist in Signature Management group. He has led a section developing computer models and software for predicting radiowave propagation in the troposphere under ducting conditions and associated surface clutter. An important element of this work is the application of atmospheric boundary layer theory to the challenging task of deriving vertical refractivity profiles from available data.

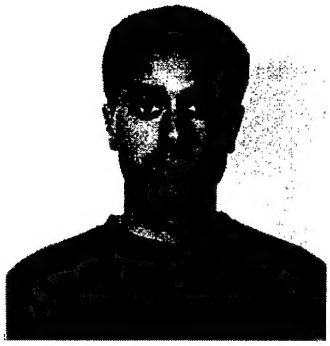

Dr Christopher P. Baker
Surveillance Systems Division

Dr Chris Baker is a Research Scientist in Surface Positioning Systems group. He as worked on atmospheric boundary later models for deriving refractivity profiles from meteorological data. He is currently involved in an operational analysis of Global Positioning Systems for the Australian Defence Force.

Contents

1. Introduction

The anomalous propagation of microwave radiation in the Atmospheric Boundary Layer (ABL) at near horizontal elevation angles due to small vertical gradients in the refractive index of the air has been described as early as 1932 (Freehafer 1988). Because the refractive index of air n is very close to unity, the quantity known as radio refractivity defined as

$$N = (n-1)\times 10^6 \tag{1}$$

is commonly used instead. The curvature of the earth is taken into account by the quantity known as modified refractivity (or refractive modulus) defined as

$$M = N + z/a_E \times 10^6, \tag{2}$$

where z is the height above the surface and a_E is the radius of the earth. When the vertical gradient of M is positive, microwave radiation curves upward; when the gradient is negative the radiation is refracted downward towards the surface and may become trapped in a surface duct.

Systems employing microwave radiation can be affected by anomalous propagation in a variety of ways. For example, Moszkowicz et al. (1994) describe how quantitative estimates of rainfall could be erroneous in the presence of anomalous propagation, unless appropriately compensated. Anderson (1995) reports how the maximum radar detection ranges of low-altitude targets over the ocean can be less than expected in the presence of surface ducting. Christophe et al. (1994) describe a series of experiments showing that the signal strength of a trans-horizon communication system can be significantly enhanced by ducting conditions.

The modelling of microwave propagation under anomalous ducting conditions has greatly improved in recent years with the development of efficient and accurate numerical solutions to the parabolic wave equation (PWE). Solutions over a plane surface were described by Dockery (1988), Craig (1998) and Craig and Levy (1991). Improved solutions have been described by Kuttler and Dockery (1991), Barrios (1992), and Dockery and Kuttler (1996). Propagation over irregular terrain has been addressed

by Levy (1990), Barrios (1994), and McArthur (1992). Improvements in computational speed have been achieved with hybrid techniques by Hitney (1992), Marcus (1992), and Levy (1995).

The results achieved with parabolic wave equation models are in good agreement with other models and with field measurements. For example, a comparison by Kuttler and Dockery (1991) of PWE results with those obtained using ray optics for a standard atmosphere and with a waveguide model for a refractivity profile with a surface duct show agreement within about 1 dB. A propagation workshop (Paulus, 1995) compared results obtained with several different PWE implementations and two sets of experimental data. The better models agreed with experiment generally within about 5 dB.

The challenge of achieving accurate propagation predictions now depends largely on obtaining sufficiently accurate descriptions of the refractivity environment through which the radiation propagates. Dockery and Goldhirsh (1995) addressed the question of what constitutes "adequate" vertical and horizontal resolution for accurate propagation assessments. Using refractivity data with a very high vertical resolution of about 1 m and an excellent horizontal resolution of about 8 km "reference" results were calculated. Then "degraded" results were obtained with data having systematically reduced vertical and horizontal resolution. A comparison of the degraded and reference results showed that an accuracy of about 5 dB could be achieved with a vertical resolution of about 6 m and a horizontal resolution of about 17 km for the cases studies. This result is based on a relatively high evaporation duct with a thickness of about 40 m. Since evaporation ducts are commonly encountered with heights down to a few metres, a vertical resolution of about 1 m may well be required close to the sea surface for accurate propagation predictions.

Because of the practical difficulty of obtaining measurements with the required vertical resolution, meteorological models of the marine atmospheric surface layer are commonly used with a few essential measurements to infer a high resolution

refractivity profile. Rogers and Paulus (1996) evaluate several evaporation duct models by comparing the propagation predictions using these models with measurements.

One such model is the Integrated Refractive Effects Prediction System (IREPS), introduced aboard US Navy ships in 1978, which uses a modified form of a surface layer model developed by Jeske (1973). This theory relies on assumptions that restrict its applicability to heights up to about 30 metres above the surface. Paulus (1985), investigating discrepancies between performance predictions and observations, concluded that errors in air-sea temperature difference observations were resulting in unrealistically high modelled duct heights. The problem was remedied by imposing an upper limit on the allowed air-sea temperature difference, which effectively limited the modelled duct heights to about 20 m.

Surface ducts are commonly observed at heights well above the 20 m height limit of the Jeske/Paulus model. An extensive series of measurements of surface duct heights over the Atlantic Ocean off the east coast of USA reported by Babin (1996) show strong seasonal and diurnal variations. Median duct heights ranged from 8 m in the morning during the January-March quarter to 40 m in the afternoon during the April-June quarter. During the latter period, some 10% of duct heights were above 100 m. Since the marine surface layer can extend to hundreds of metres above the sea surface, an adequate surface layer model should be valid for hundreds not just tens of metres above the surface.

A more general approach to modelling the marine atmospheric surface layer is described by Liu Katsaros and Businger (1979), which will be called the LKB model. Like the Jeske/Paulus model, the LKB model requires as input data: wind speed, air temperature, and relative humidity (or a related moisture parameter) at known heights above the surface together with sea surface temperature and atmospheric pressure. The LKB model uses these data in similarity relations to determine the momentum, heat, and moisture fluxes, which are approximately independent of height in the

surface layer, and thence the vertical profiles of wind speed, temperature and specific humidity.

The vertical profile of radio refractivity can then be derived from the profiles of temperature and specific humidity using the relation (Bean and Dutton, 1968 and ITU-R, 1994):

$$N = \frac{77.6}{T}\left(P + 4810\frac{e}{T}\right), \tag{3}$$

where T is the absolute temperature (K), P is the atmospheric pressure (hPa), and e is the water vapour pressure (hPa).

The present paper develops the similarity theory of the atmospheric surface layer further by identifying where the surface layer blends into the mixed layer, which lies above it and which forms the bulk of the atmospheric boundary layer. The paper also describes a method for assimilating multiple sets of meteorological measurements to improve the accuracy of derived surface layer fluxes. Importantly, the meteorological measurements need not be in the surface layer; they can also be in the mixed layer, or both. This allows both individual measurements (eg from an instrumented buoy) and radiosonde soundings to be assimilated to achieve an optimal estimate of the refractivity profile in both the surface and mixed layers.

2. Refractivity Profile Model

The refractivity profile model described in this paper applies to the Atmospheric Boundary Layer (ABL), which Stull (1988) defines as "that part of the troposphere that is directly influenced by the presence of the earth's surface, and responds to surface forcings with a timescale of about an hour or less," and which has a thickness varying from hundreds to thousands of metres. The model covers both the *surface layer*, which comprises the bottom 5 to 10% of the ABL where the turbulent fluxes and stress are approximately independent of height, and the *mixed layer*, which occupies the middle 80% or so of the ABL, above the surface layer.

2.1 Surface Layer

Within the surface layer, Monin-Obukhov similarity theory is used to describe the dependence of wind speed U, virtual potential temperature Θ_v and mixing ratio Q on height z. Virtual temperature, which is the temperature of dry air that would have the same density as moist air at the same pressure, is useful in buoyancy models and is approximately given by

$$T_v = T(1 + 0.61Q), \tag{4}$$

where T is measured in Kelvin and Q is in g/g. Potential temperature Θ is the temperature that a parcel of air would attain if its pressure were brought adiabatically to a reference pressure P_{ref} (usually 1000 hPa), ie

$$\Theta = T\left(P_{ref}/P\right)^{R/C_p}, \tag{5}$$

where R is the universal gas constant and C_p is the specific heat of air at constant pressure.

Following Arya (1988), with two changes described below, the vertical profiles are given by

$$U(z) = \frac{u_*}{k}\left[\ln(1 + z/z_{0m}) - \psi_m(z/L)\right], \tag{6}$$

$$\Delta\Theta_v(z) \equiv \Theta_v - \Theta_{v0} = \frac{\theta_*}{k}\left[\ln(1+z/z_{0h}) - \psi_h(z/L)\right], \tag{7}$$

$$\Delta Q(z) \equiv Q - Q_0 = \frac{q_*}{k}\left[\ln(1+z/z_{0h}) - \psi_h(z/L)\right]. \tag{8}$$

The two changes are: (a) that the argument of the logarithm is $(1+z/z_0)$ instead of (z/z_0) in order to ensure that all three functions vanish at zero height and (b) that different values of z_0 are assumed to be associated with wind speed, z_{0m}, and with temperature and moisture, z_{0h}. In these equations, the parameters u_*, θ_*, and q_* are scales for wind speed, temperature and moisture respectively, k is the von Karman constant which has a value of about 0.40, and the Obukhov length L, which is the characteristic length for dynamic turbulence in the surface layer, is negative under unstable conditions and positive under stable conditions and its magnitude typically ranges from a few metres to hundreds of metres. It is defined by

$$L = \frac{T_{v0}}{kg}\frac{{u_*}^2}{\theta_*}, \tag{9}$$

where T_{v0} is the virtual temperature at the surface and g is the gravitational acceleration. The dependence of the Obukhov Length on wind speed scale or friction velocity, u_*, and temperature scale, θ_*, is shown in Fig. 1.

The ψ functions, which account for departures of the surface layer from the neutral stability condition, are given by

$$\psi_m\left(\frac{z}{L}\right) = \begin{cases} -5\dfrac{z}{L}, & for\ \dfrac{z}{L} \geq 0, \\ \ln\left[\left(\dfrac{1+x^2}{2}\right)\left(\dfrac{1+x}{2}\right)^2\right] - 2\arctan x + \dfrac{\pi}{2}, & for\ \dfrac{z}{L} < 0, \end{cases} \tag{10}$$

$$\psi_h\left(\frac{z}{L}\right) = \begin{cases} -5\dfrac{z}{L}, & for\ \dfrac{z}{L} \geq 0, \\ 2\ln\left(\dfrac{1+x^2}{2}\right), & for\ \dfrac{z}{L} < 0, \end{cases} \tag{11}$$

where $x = (1-15z/L)^{1/4}$.

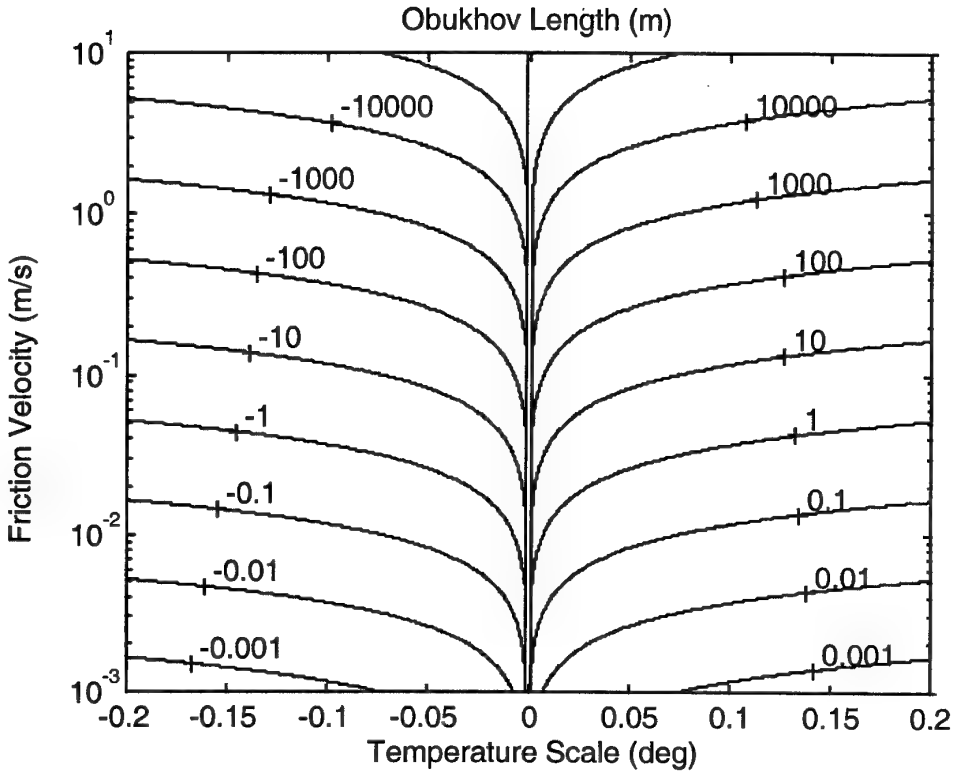

Figure 1: The dependence of the Obukhov Length on friction velocity, u_*, and temperature scale, θ_*.

Equations (6), (7) and (8) provide a set of three non-linear functions expressing the three observables U, $\Delta\Theta_v$ and ΔQ in terms of the five unknowns parameters u_*, θ_*, q_*, z_{0m} and z_{0h} that can be written in the form

$$U(z) = F_U\left(z, u_*, \theta_*, z_{0m}\right), \tag{12}$$

$$\Delta\Theta_v(z) = F_\Theta\left(z, u_*, \theta_*, z_{0h}\right), \tag{13}$$

$$\Delta Q(z) = F_Q\left(z, u_*, \theta_*, q_*, z_{0h}\right). \tag{14}$$

Because the parameter q_* occurs only in the equation for ΔQ, it is most convenient to consider first the solution of the equations for U and $\Delta\Theta_v$. Since these two equations have four unknowns, two additional equations are needed. Over sea, Charnock's

relation (Charnock 1955) is assumed, giving the following relationship for the roughness length for momentum transfer:

$$z_{0m} = a_c u_*^{\,2} / g, \tag{15}$$

where Charnock's constant $a_c \approx 0.018$ (Arya 1988: p 204). Over land, an empirical relation is often assumed between roughness length and topographic height, such as

$$z_{0m} = 0.001(\text{topographic height})^{0.7} \tag{16}$$

which is based on the table of typical values of roughness length reproduced by Arya (1988: p 149). The final equation needed for the solution is

$$z_{0h} = a_h z_{0m}, \tag{17}$$

where a_h is an experimentally determined parameter relating the two roughness lengths.

For a surface layer over sea, Fig. 2 shows the forms of the expressions for U and $\Delta\Theta_v$ at a height of 10 m given by equations (12) and (13) respectively. Fig. 2a shows that, for a given value of temperature scale (θ_*), the wind speed increases with friction velocity (u_*) as would be expected, except when $\theta_*>0$ and u_* is small where the theory predicts a spurious decrease of wind speed with friction velocity . Fig. 2b shows that, for a given value of friction velocity, the virtual potential temperature difference $\Delta\Theta_v$ increases with temperature scale as expected.

Over land, Fig. 3 shows the forms of the expressions for U and $\Delta\Theta_v$ again at a height of 10 m and with roughness length values $z_{0h} = z_{0m} = 0.1$ m. Fig. 3a shows the expected increasing wind speed with friction velocity for values of u_* greater than about 0.1 but the theory predicts a spurious decrease of wind speed with friction velocity for both positive and negative temperature scales at smaller values of the friction velocity. Fig. 3b shows the expected increasing $\Delta\Theta_v$ with temperature scale, except when the temperature scale is negative and the friction velocity is small.

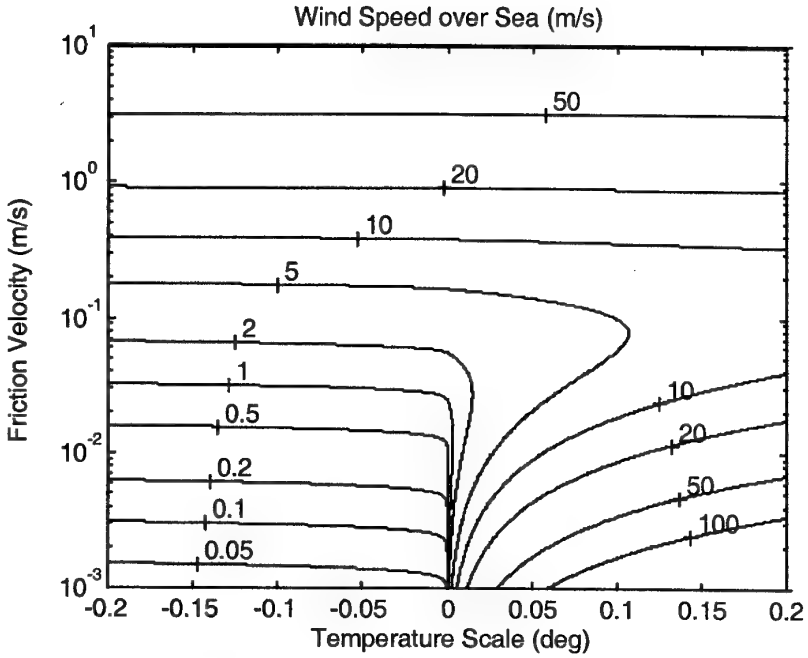

(a)

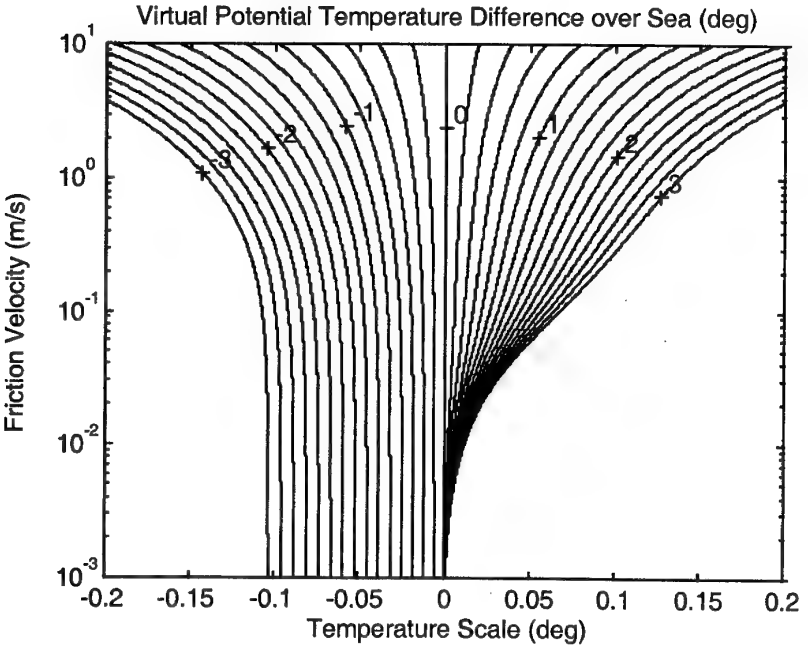

(b)

Figure 2: Contour plots showing the dependence over sea of (a) wind speed and (b) virtual potential temperature difference at a height of 10 metres on friction velocity (u_*) and temperature scale (θ_*).

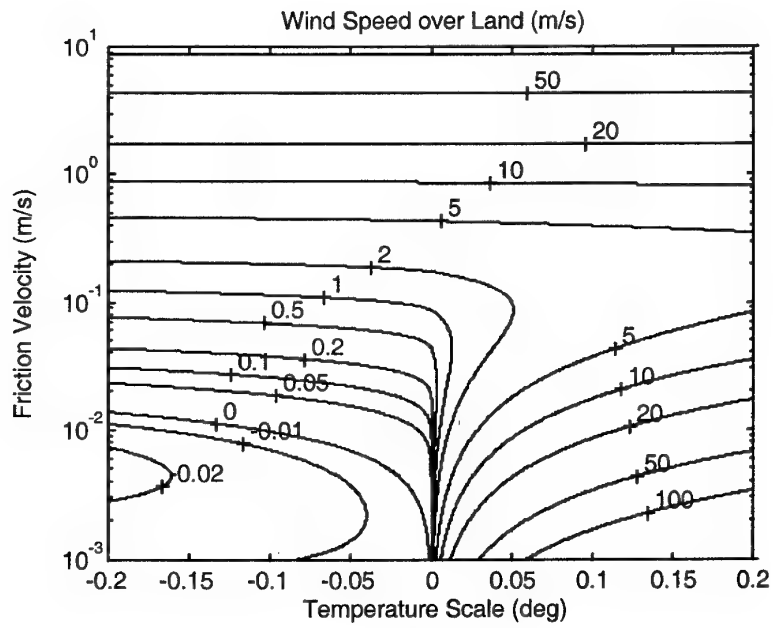

(a)

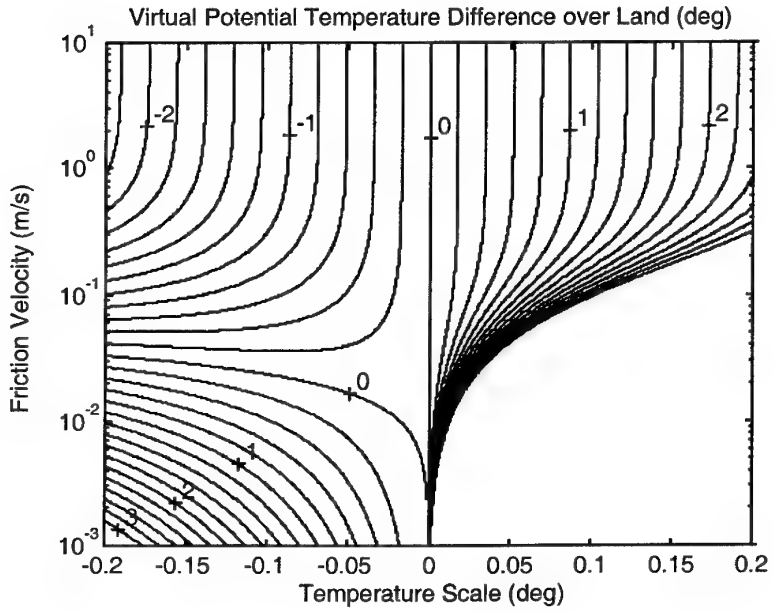

(b)

Figure 3: Contour plots showing the dependence over land of (a) wind speed and (b) virtual potential temperature difference at a height of 10 metres on friction velocity (u_*) and temperature scale (θ_*).

2.2 Mixed Layer

The mixed layer is characterised by intense vertical mixing which tends to leave conserved variables such as virtual potential temperature and mixing ratio nearly constant in height. Consequently, it is assumed that wind speed, virtual potential temperature and mixing ratio have values throughout the mixed layer equal to those at the top of the surface layer, namely

$$U(z) = F_U\left(z_s, u_*, \theta_*, z_{0m}\right), \quad z_S \le z \le z_i \tag{18}$$

$$\Delta\Theta_v(z) = F_\Theta\left(z_s, u_*, \theta_*, z_{0h}\right), \quad z_S \le z \le z_i \tag{19}$$

$$\Delta Q(z) = F_Q\left(z_s, u_*, \theta_*, q_*, z_{0h}\right), \quad z_S \le z \le z_i \tag{20}$$

where z_s is the height of the surface layer and z_i is the height of the ABL.

2.3 Surface layer height

The critical parameter in matching the models for the surface and mixed layers is the surface layer height. A reasonable physical assumption for the surface layer is that the wind speed at a given height and the friction velocity are positively correlated. In other words, the wind speed at a given height is assumed to increase monotonically with friction velocity, that is

$$\partial U / \partial u_* \ge 0. \tag{21}$$

Likewise, the virtual potential temperature difference at a given height and the temperature scale are assumed to be positively correlated, which leads to the requirement that

$$\partial\Delta\Theta_v / \partial\theta_* \ge 0. \tag{22}$$

Figures 4 and 5 show the values of these partial derivatives over sea and over land respectively, corresponding to the plots of U and $\Delta\Theta_v$ illustrated in Figs 2 and 3. It can be seen that conditions (21) and (22) hold over only part of the (θ_*, u_*) domain. Over sea, Fig. 4 shows that $\partial U / \partial u_*$ becomes negative for positive temperature scale and

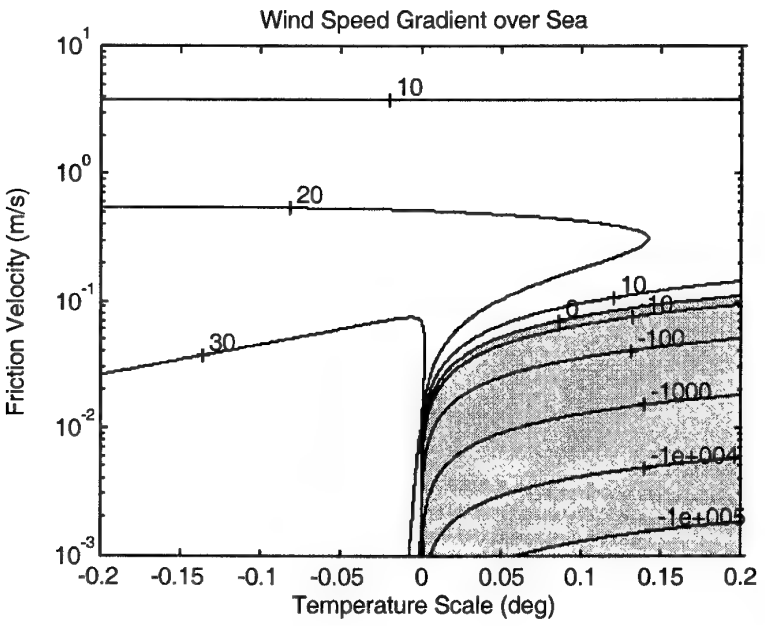

(a)

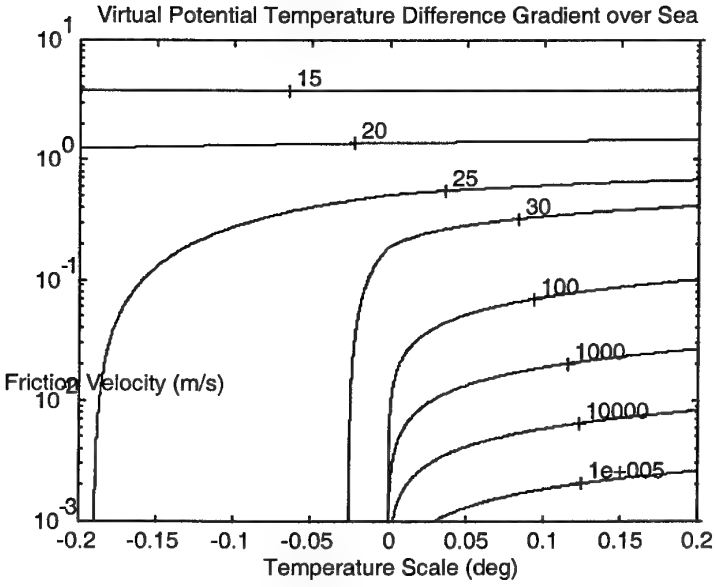

(b)

Figure 4: Contour plots showing the dependence over sea of (a) wind speed gradient with respect to friction velocity ($\partial U / \partial u_*$) and (b) virtual potential temperature difference gradient with respect to temperature scale ($\partial \Delta\Theta / \partial \theta_*$) at a height of 10 metres on friction velocity (u_*) and temperature scale (θ_*). The shading indicates the domain with a negative wind speed gradient.

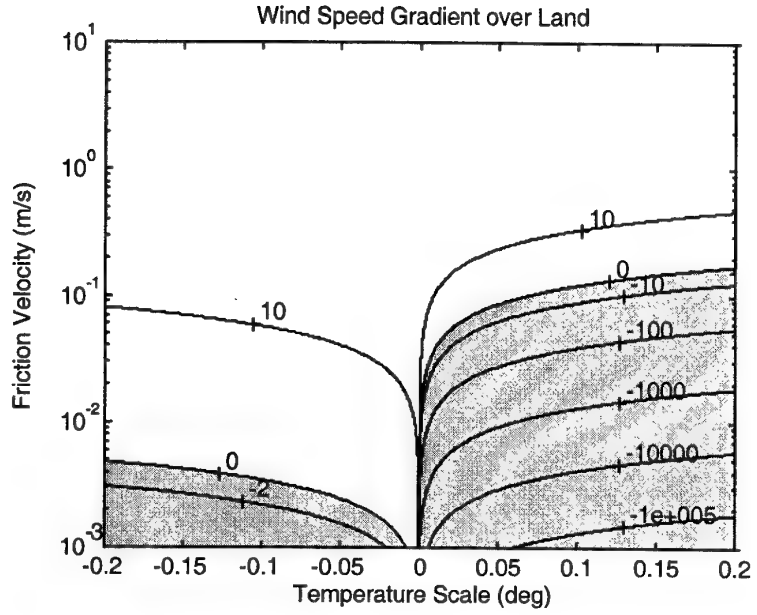

(a)

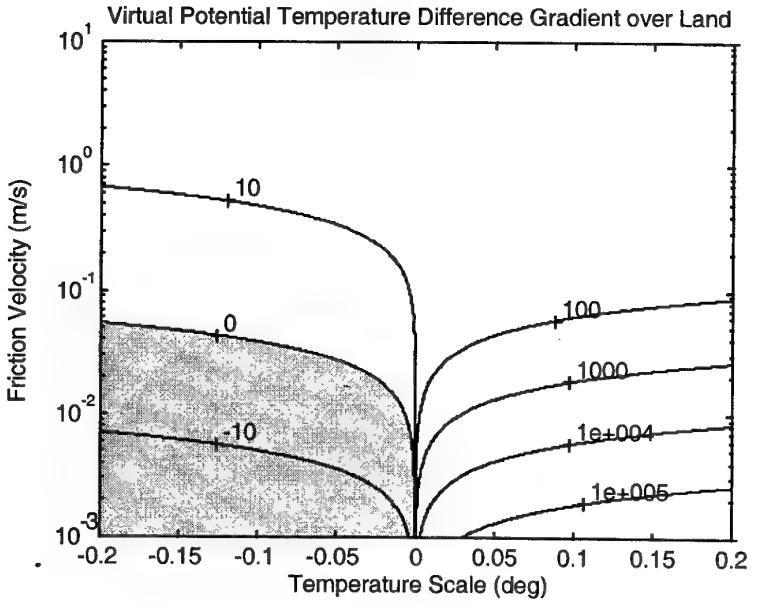

(b)

Figure 5: Contour plots showing the dependence over land of (a) wind speed gradient with respect to friction velocity ($\partial U / \partial u_*$) and (b) virtual potential temperature difference gradient with respect to temperature scale ($\partial \Delta\Theta / \partial \theta_*$) at a height of 10 metres on friction velocity (u_*) and temperature scale (θ_*). The shading indicates the domains with negative gradients.

small friction velocity. Over land, Fig. 5(a) shows that $\partial U / \partial u_*$ becomes negative for both positive and negative temperature scale and small friction velocity and Fig 5(b) shows that $\partial \Delta\Theta / \partial \theta_*$ also becomes negative for negative temperature scale and small friction velocity. The limiting cases, where the partial derivatives in equations (21) and (22) vanish, are assumed to define the limit of validity of the surface layer model and hence the surface layer height.

Over sea, where the roughness length for wind depends on friction velocity through the Charnock relation (equation 14), both stable (positive Obukhov length) and unstable (negative Obukhov length) conditions need to be considered. In the stable case, equation (22) is always satisfied and the condition that $\partial U / \partial u_* = 0$ at $z = z_s$ can be shown to be

$$\ln\left(1+\frac{gz_s}{a_c u_*^{\,2}}\right)-\frac{2}{1+(a_c u_*^{\,2}/gz_s)}-5\frac{kgz_s\theta_*}{T_{v0}u_*^{\,2}}=0, \quad \text{for L} > 0, \tag{23}$$

which can be solved to yield z_s / L as a function of θ_* and the result is shown in Fig. 6. This result for stable conditions, that the surface layer height typically lies between two and three times L, is consistent with the statement by Arya (1988) that the Monin-Obukhov similarity functions are based on data approximately covering the stability range

$$-5 < z_s / L < 2. \tag{24}$$

For unstable conditions over sea, the partial derivatives (21) and (22) are always positive and the limit given by Arya is adopted, namely

$$z_s / L = -5. \tag{25}$$

When the surface layer height over sea as defined above is taken into account, the dependences of wind speed and virtual potential temperature on friction velocity and temperature scale as are shown in Fig 7. It is evident from the figure that the two partial derivative conditions in (21) and (22) are satisfied and unique solutions for u_* and θ_* can be obtained from measured values of U and $\Delta\Theta_v$.

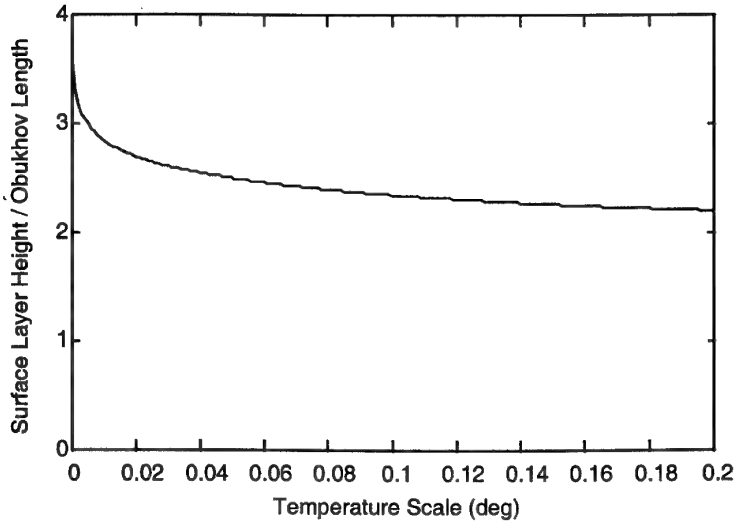

Figure 6: Dependence over sea of relative surface layer height, z_s / L, on temperature scale.

Over land, where the roughness lengths for wind and heat are constant, both stable and unstable conditions again need consideration. For stable case, equation (22) is always satisfied and the condition that $\partial U / \partial u_* = 0$ at $z = z_s$ yields

$$\ln\left(1+\frac{z_s}{z_{om}}\right)-5\frac{z_s}{L}=0, \tag{26}$$

which results in the dependence of z_s / L on L and z_{om} shown in Fig. 8. It can be seen that $z_s / L \geq 1$ for small L only if the roughness length is small enough. For the unstable case, the surface layer height is again assumed to be -5L, as in equation (25) and the conditions (21) and (22) are used to constrain the roughness lengths, as described below.

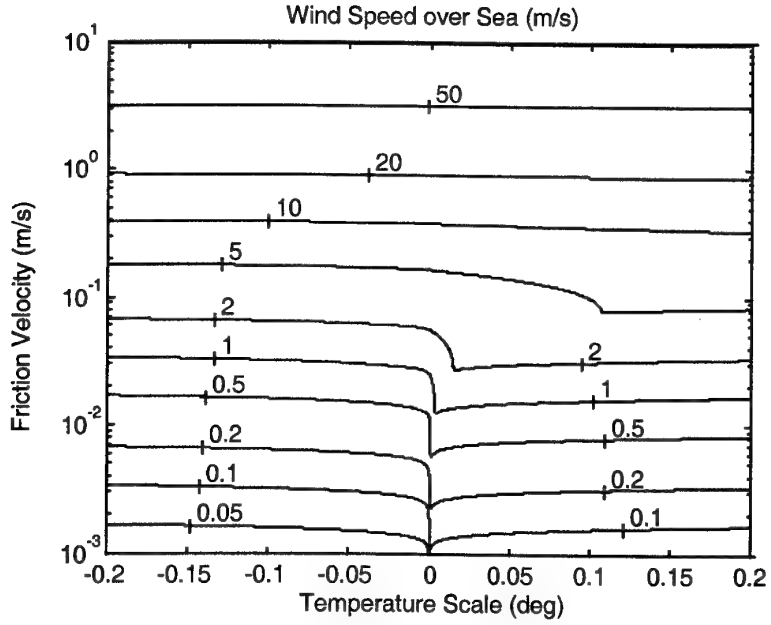

(a)

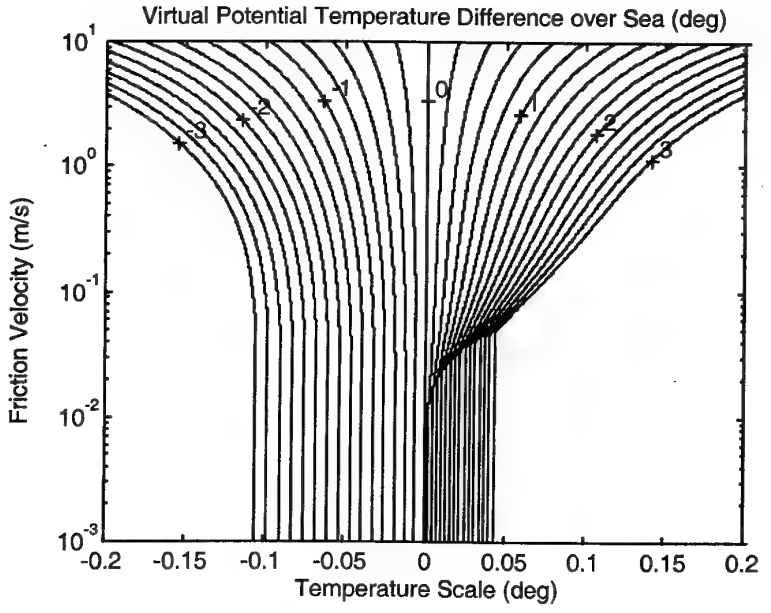

(b)

Figure 7: Contour plots showing the dependence over sea of (a) wind speed and (b) virtual potential temperature difference at a height of 10 metres on friction velocity (u_*) and temperature scale (θ_*), when the surface layer height has been taken into account.

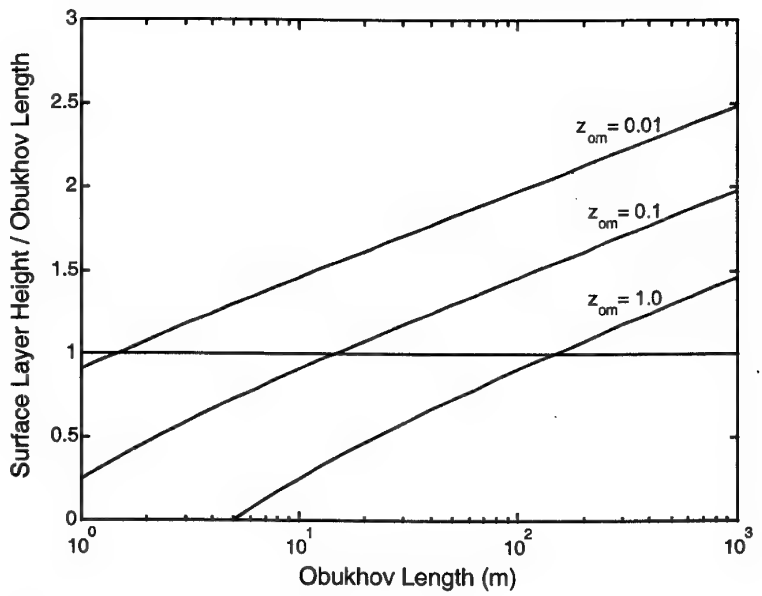

Figure 8: Dependence over land of relative surface layer height, z_s / L, on Obukhov length, L, *and roughness length for wind* z_{om}.

2.4 Roughness lengths

Over land, the partial derivative conditions (21) and (22) have implications for the roughness lengths z_{om} and z_{oh}. For the stable case, the inequality related to equation (26) can be re-written as

$$z_{om} \leq \frac{z_s}{\exp(5z_s / L) - 1}, \tag{27}$$

which imposes a maximum acceptable value on the roughness length for wind that depends on the surface layer height. If the empirically estimated roughness length for wind, derived from a relation such as (16), exceeds the maximum acceptable value given by equation (27), it is assumed to be incorrect and z_{om} is assigned a new value equal to the right hand side of equation (27). This lower value of roughness length for wind ensures that condition (21) is satisfied.

For the unstable case, condition (22) becomes

$$\ln\left(1+\frac{z_s}{z_{oh}}\right) - 2\ln\left(\frac{1+x_s^{\,2}}{2}\right) + \frac{15z_s}{Lx_s^{\,2}\left(1+x_s^{\,2}\right)} \geq 0, \tag{28}$$

where

$$x_s = \left(1-15\frac{z_s}{L}\right)^{1/4}. \tag{29}$$

With the surface layer height assumed to be -5L, this condition is satisfied when

$$z_{oh} \leq -L/11.3. \tag{30}$$

If the empirically estimated roughness length for heat exceeds the maximum acceptable value given by equation (30), it is assumed to be incorrect and z_{oh} is assigned a new value equal to the right hand side of equation (30). This lower value of roughness length for heat ensures that condition (22) is satisfied.

Tests show that conditions (27) and (30) are not strong enough to prevent poor conditioning of the equations to be solved over land. Robust solutions are obtained when the roughness lengths are required to satisfy the following slightly stronger conditions. The roughness length for wind are required to satisfy, in the stable case,

$$z_{om} \le \frac{z_s}{\exp\left(3.5 + 5z_s / L\right)}, \tag{31a}$$

and, in the unstable case,

$$z_{om} \le \frac{z_s}{\exp\left(3.5 - 0.2z_s / L\right)}. \tag{31b}$$

The roughness length for heat are required to satisfy, in the both stable and unstable cases,

$$z_{oh} \le |L| / 60. \tag{32}$$

Over land, when the surface layer height defined in the previous section is used in conjunction with the conditions on the roughness lengths in (31) and (32), the dependences of wind speed and virtual potential temperature on friction velocity and temperature scale as are shown in Fig 9. It is again evident from the figure that the two partial derivative conditions in (21) and (22) are satisfied and unique solutions for u_* and θ_* can be obtained from measured values of U and $\Delta\Theta_v$.

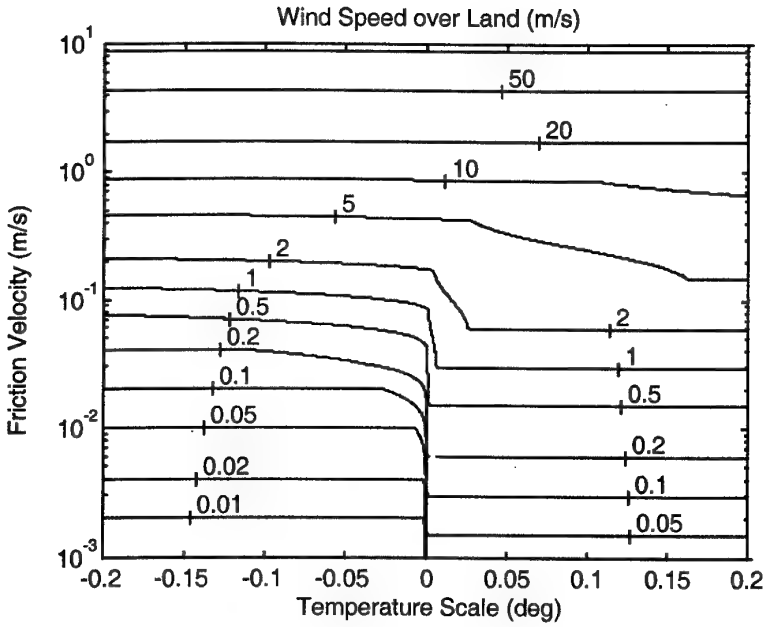

(a)

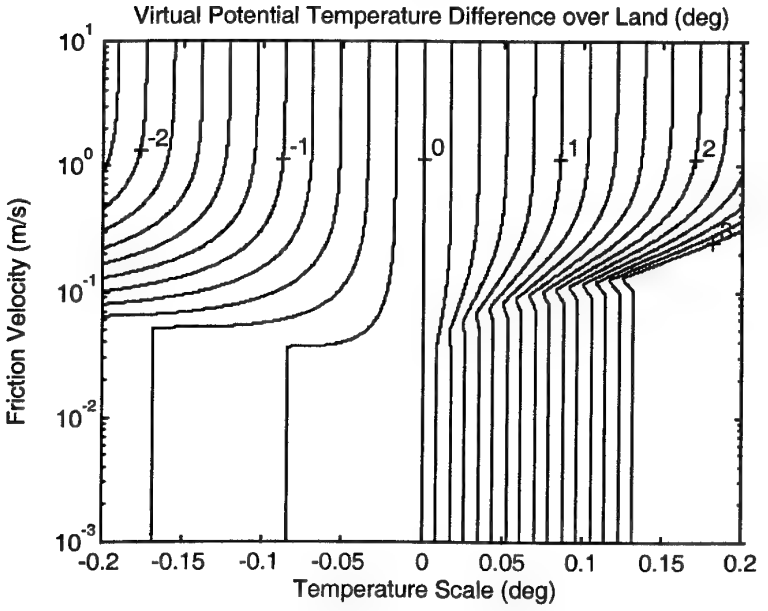

(b)

Figure 9: Contour plots showing the dependence over land of (a) wind speed and (b) virtual potential temperature difference at a height of 10 metres on friction velocity (u_*) and temperature scale (θ_*), when the surface layer height has been taken into account.

3. Data Assimilation

Air temperature and moisture data are commonly measured at multiple heights, for example by radiosondes, whereas the theory described in the previous section uses only a single pair of air temperature and moisture measurements - together with wind speed and surface temperature and moisture data. Since the derived wind speed, temperature and moisture scales u_*, θ_*, and q_* are proportional to the surface fluxes of stress, sensible heat and latent heat respectively, they are independent of the height of the air temperature and moisture measurements. Optimal estimates of these scales can therefore be obtained from weighted averages of estimates derived from measurements at different heights.

Suppose that u_{*j} and θ_{*j} are estimates of u_* and θ_* derived from wind speed and temperature measurements at height z_j, with associated experimental errors $e_u(z_j)$ and $e_\theta(z_j)$ respectively. The best estimates of u_* and θ_* are then given by the weighted means

$$u_* = \sum_j w_{uj} u_{*j} \quad \text{and} \quad \theta_* = \sum_j w_{\theta j} \theta_{*j} \,, \tag{33}$$

where

$$w_{uj} = \frac{1/e_u(z_j)^2}{\sum_j 1/e_u(z_j)^2} \quad \text{and} \quad w_{\theta j} = \frac{1/e_\theta(z_j)^2}{\sum_j 1/e_\theta(z_j)^2} \,. \tag{34}$$

3.1 Sensitivity analysis

The dependence of the error functions $e_u(z)$ and $e_\theta(z)$ on height was determined from a sensitivity analysis of the solution over sea. First, assumed values of u_*, θ_* and z were used to calculate the corresponding values of $U(z)$ and $\Delta\Theta_v(z)$. Then, eight perturbed combinations of wind speed, air temperature and height were obtained by adding and subtracting assumed errors of 0.1 m/s, 0.1 K, and 0.1 m respectively and the equations

solved to yield eight perturbed estimates of u_* and θ_*, from which the bias and RMS errors were obtained. This was repeated for a representative sample of assumed values of u_* and θ_* covering the domain $0.01 < u_* < 10$ and $-0.2 < \theta_* < 0.2$ and average bias and RMS errors were obtained for the assumed data height. Heights ranging from 1 to 1000 metres were analysed in this way and the results are given in Figs 10 and 11.

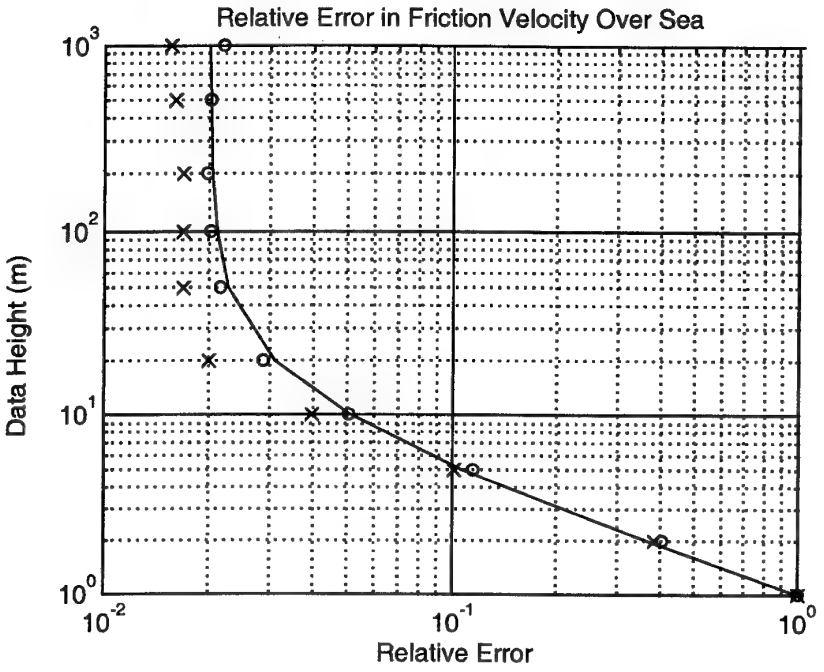

Figure 10: The dependence on height of relative errors in friction velocity u_* over sea. The symbols represent bias (x) and RMS error (o) and the line is an empirical curve fitted to the RMS error.

It is evident from these results that the errors decrease strongly with height, particularly in the first 10 metres or so above the surface. The error in friction velocity decreases very strongly with height. Empirical curves fitted to the RMS error data are

$$e_u(z) = 0.98z^{-3/2} + 0.02 \quad \text{and} \quad e_\theta(z) = 0.46z^{-1.2} + 0.54z^{-0.07}. \tag{35}$$

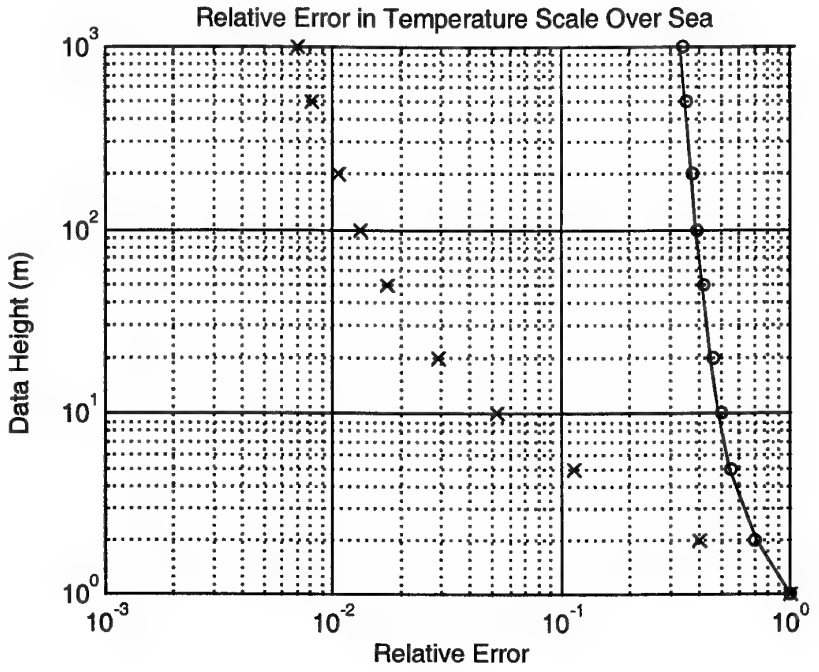

Figure 11: The dependence on height of relative errors in temperature scale θ_* over sea. The symbols represent bias (x) and RMS error (o) and the line is an empirical curve fitted to the RMS error.

3.2 Experimental data

The techniques described in this paper were applied to a set of data obtained during the TOGA (Tropical Ocean Global Atmosphere) COARE (Coupled Ocean-Atmosphere Response Experiment) program in the tropical western Pacific Ocean during 1992 (World Climate Research Program, 1990; Webster and Lukas, 1992). The measurements were made over the sea at the location 156°E, 2°S using instrumentation attached to a floating buoy. The wind speed was measured at a height of 8 m above the sea surface and measurements of pressure, temperature, and relative humidity were made at multiple heights up to about 5 m.

After conversion of the temperature and moisture data to virtual potential temperature and mixing ratio, the similarity equations were solved using two values of the roughness ratio parameter a_h, defined in eq. (17), namely 1 and 1000. The resulting profiles of virtual potential temperature and mixing ratio are shown in Figs 12(a) and 12(b). The associated profiles of modified refractivity, determined using eqs (2) and (3), are shown in Fig. 12(c). It is evident from the figure that the use of equal roughness lengths for wind and heat produces a poor fit to the data. When the roughness length for heat is assumed to be 1000 times that for wind, a good fit to the observations is achieved for mixing ratio and modified refractivity.

The value of the roughness ratio makes a significant difference to the whole shape of the modified refractivity profile. In particular, the value of the associated duct height, which is defined as the height of the local minimum in the modified refractivity profile, changes from 10 m when equal roughness lengths are assumed to 17 m when a roughness ratio of 1000 is assumed.

The generalisation of allowing the roughness lengths for wind and heat to differ is justified theoretically because different physical processes are responsible for transfer of momentum and heat very close to the surface. Moreover, this generalisation resolves the discrepancy between the measurements and model reported by Baker *et al.* (1996) when equal roughness lengths were assumed. Clearly, analysis of many experimentally measured profiles of temperature and moisture is needed to establish the best value of the roughness ratio.

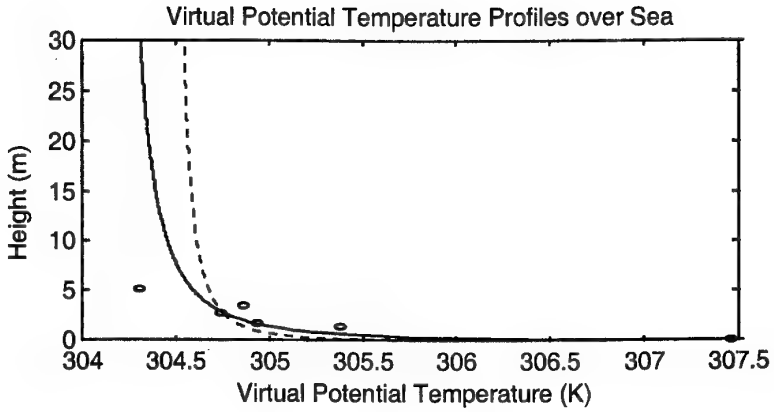

(a)

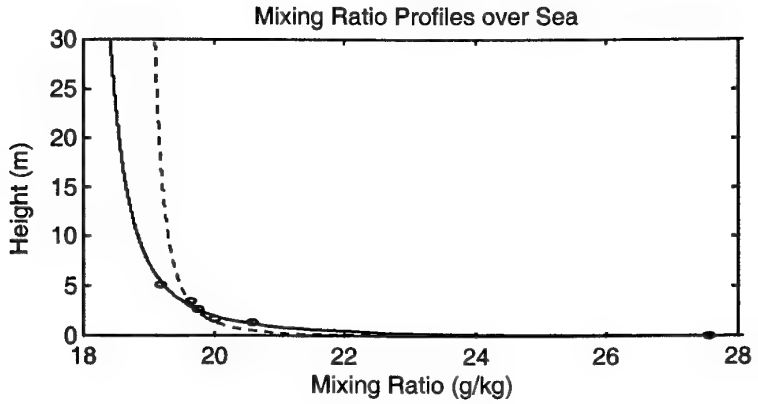

(b)

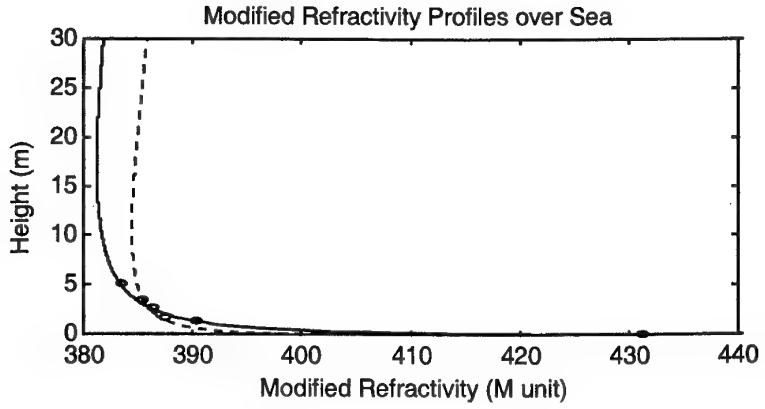

(c)

Figure 12: Profiles of (a) virtual potential temperature, (b) mixing ratio, and (c) modified refractivity using equal roughness lengths for wind and heat (dashed line) and a roughness ratio of 1000 (solid line); the experimental measurements are shown as small ovals (o).

4. Conclusion

The theoretical description of the Atmospheric Boundary Layer (ABL) developed in this paper merges the similarity theory of the surface layer with the properties of the mixed layer. The result is a set of equations that yield robust solutions under a wide variety of conditions, using meteorological data at any height in the ABL. It is not necessary to know in advance whether the measurement height is in the surface layer or in the mixed layer above it, and the equations yield robust solutions over both sea and land.

A significant advantage of this model over models limited to the surface layer is that data from meteorological analysis and forecast models can be used to determine the refractivity profiles that govern evaporation ducts. This vastly extends the geographical extent of knowledge of evaporation duct conditions from local measurements in the vicinity of ships to coverage of the vast oceans of the globe.

This approach also enables the optimal assimilation of meteorological data from a variety of heights in the ABL. A sensitivity analysis of the equations shows that errors in the estimated parameters increase markedly at low heights, particularly below about 10 m.

Application of the theory to one set of data over sea shows that a significant improvement in the fit to the data is achieved when the roughness length for heat is assumed to be much greater than the roughness length for wind. Clearly, further work of analysing a large data set is needed to clarify the relationship between the two roughness lengths.

Acknowledgments. The authors are indebted to Dr Andrew Kulessa of DSTO Electronic Warfare Division for supplying the experimental data from the TOGA COARE program. They also thank Messrs Michael Woodcock and Nick Wilson contracted from Aspect Computing Pty Ltd for their assistance analysing the data.

5. References

Anderson, K. D., 1995: Radar detection of low-altitude targets in a maritime environment. *IEEE Trans. Antennas Propagat.*, **43**, 609-613.

Arya, S. P., 1988: *Introduction to Micrometeorology*, Academic Press, 307 pp.

Babin, S. M. 1996: Surface duct height distributions for Wallops Island, Virginia, 1985-1994, *J. Appl. Meteor.*, **35**, 86-93.

Baker, C.P., Phillips, D.M. and McDonald, D.M., 1996: *Implementation of Boundary Layer Theory for the Determination of Atmospheric Refractivity Profiles*, DSTO-TR-0421.

Barrios, A. E., 1992: Parabolic equation modeling in horizontally inhomogeneous environments. *IEEE Trans. Antennas Propagat.*, **40**, 791-797.

Barrios, A. E., 1994: A terrain parabolic equation model for propagation in the troposphere. *IEEE Trans. Antennas Propagat.*, **42**, 90-98.

Bean, B. R. and Dutton, E. J. , 1968: *Radio Meteorology*, Dover Publications, 435 pp.

Charnock, H., 1955: Wind stress on a water surface. *Quart. J. Roy. Meteor. Soc.*, **81**, 639-640.

Christophe, F., Douchin, N. , Hurtaud, Y. , Dion, D., Makaraschka, R., Heemskerk, H. and Anderson, K., 1995: Overview of NATO/AC 243/Panel 3 activities concerning radiowave propagation in coastal environments. *AGARD Conference Proceedings 567, Propagation Assessment in Coastal Environments*, Bremerhafen, Germany 19-22 September 1994, 27.1-27.9.

Craig, K.H. 1988: Propagation modelling in the troposphere: parabolic equation method. *Electron. Lett.*, **24**, 1136-1139.

Craig, K. H. and Levy, M. F., 1991: Parabolic equation modelling of the effects of multipath and ducting on radar systems. *IEE Proc.-F*, **138**, 153-162.

Dockery, G. D., 1988: Modeling electromagnetic wave propagation in the troposphere using the parabolic equation. *IEEE Trans. Antennas Propagat.*, **36**, 1464-1470.

Dockery, G. D. and Goldhirsh, J., 1995: Atmospheric data resolution requirements for propagation assessment: case studies of range-dependent coastal environments. *AGARD Conference Proceedings 567, Propagation Assessment in Coastal Environments*, Bremerhafen, Germany 19-22 September 1994, 7.1-7.12.

Dockery, G. D. and Kuttler, J. R., 1996: An improved impedance-boundary algorithm for Fourier split-step solutions of the parabolic wave equation. *IEEE Trans. Antennas Propagat.*, **44**, 1592-1599.

Freehafer, J. E., 1988: Tropospheric refraction. *Propagation of Short Radio Waves*, D. E. Kerr, Ed., Peninsula Publishing, 9-22.

Hitney, H. V., 1992: Hybrid ray optics and parabolic equation methods for radar propagation modeling. *Proc. IEE Int. Conf. Radar*, Brighton, U.K., 12-13 October 1992, 58-61.

ITU-R, 1994: The radio refractive index: its formula and refractivity data, in *Propagation in Non-ionized Media*, ITU-R Recommendations, 1994 PN Series volume, 206-213.

Jeske, H. 1973: State and limits of prediction methods of radar wave propagation conditions over sea, in *Modern Topics in Microwave Propagation and Air-Sea Interaction: Proc. NATO Advanced Study Institute*, A. Zancla, Ed., Sorrento, Italy, 5-14 June, 131-148.

Kuttler, J. R. and Dockery, G. D., 1991: Theoretical description of the parabolic approximation/Fourier split-step method of representing electromagnetic propagation in the troposphere. *Radio Sci.*, **26**, 381-393.

Levy, M.F., 1990: Parabolic equation modeling over irregular terrain. *Electron. Lett.*, **26**, 1153-1155.

Levy, M.F., 1995: Horizontal parabolic equation solution of radiowave propagation problems on large domains. *IEEE Trans. Antennas Propagat.*, **43**, 137-144.

Liu, W. T., K. B. Katsaros, and J. A. Businger, 1979: Bulk parameterization of air-sea exchanges of heat and water vapour including the molecular constraints at the interface. *J. Atmos. Sci.*, **36**, 1722-1735.

Marcus, S. H., 1992: A hybrid (finite difference-surface Green's function) method for computing transmission losses in an inhomogeneous atmosphere over irregular terrain. *IEEE Trans. Antennas Propagat.*, **40**, 1451-1458.

McArthur, R. J., 1992: Propagation modeling over irregular terrain using the split-step parabolic equation method. *Proc. IEE Int. Conf. Radar*, Brighton, U.K., 12-13 October 1992, 54-57.

Moszkowicz, S., G. J. Ciach, and W. F. Krajewski, 1994: Statistical detection of anomalous propagation in radar reflectivity patterns. *J. Atmos. Ocean Technol.*, **11**, 1026-1034.

Paulus, R. A., 1985: Practical application of an evaporation duct model. *Radio Sci.*, **20**, 887-896.

Paulus, R., 1995: *Proceedings of the Electromagnetic Propagation Workshop*, Naval Command Control and Ocean Surveillance Center Technical Document 2891, 451 & 502.

Rogers, L. T. and R. A. Paulus, 1996: Measured performance of evaporation duct models. *Battlespace Atmospherics Conference*, 3-5 December 1996, NRad, San Diego, CA.

Stull, R. B., 1988: *An Introduction to Boundary Layer Meteorology*, Kluwer Academic Publishers, 666 pp.

Webster, P.J. and R. Lukas, 1992: TOGA COARE: The coupled ocean atmosphere response experiment, *Bull. Am. Meteorol. Soc.*, **73**, 1377-1416.

World Climate Research Program, 1990: Scientific plan for the TOGA Coupled Ocean-Atmosphere Response Experiment, *World Clim. Res. Program Publ. Ser., WMO/TD-64*, **3**, addendum, World Meteorol. Organ., Geneva, 105 pp.

DISTRIBUTION LIST

Refractivity Profile Assimilation Model for the Atmospheric Boundary Layer

D. M. Phillips and C P. Baker

AUSTRALIA

DEFENCE ORGANISATION

Task Sponsor

Chief of Surveillance Systems Division	1 copy

S&T Program

Chief Defence Scientist FAS Science Policy AS Science Corporate Management	1 shared copy
Director General Science Policy Development	Doc Data Sheet only
Counsellor Defence Science, London	Doc Data Sheet only
Counsellor Defence Science, Washington	Doc Data Sheet only
Scientific Adviser to MRDC Thailand	Doc Data Sheet only
Scientific Adviser Policy and Command	1 copy
Navy Scientific Adviser	1 copy
Scientific Adviser - Army	Doc Data Sheet and distribution list only
Air Force Scientific Adviser	1 copy
Director Trials	Doc Data Sheet only

Aeronautical and Maritime Research Laboratory

Director	Doc Data Sheet only
Chief of Weapons Systems Division	1 copy

Electronics and Surveillance Research Laboratory

Director	1 copy
Chief of Electronic Warfare Division	1 copy
Chief of Communications Division	1 copy
Research RF EW, EWD	1 copy
Research Leader Maritime Surveillance, SSD	1 copy
Head of System Integration and Modelling Group, EWD	1 copy
Head of Signature Management Group, SSD	1 copy
A.S. Kulessa, EWD	1 copy
B.J. Kachoyan, MOD	1 copy
J.A. Hermann, SSD	1 copy
D.M. McDonald, SSD	1 copy
Author: D.M. Phillips	3 copies
Author: C.P. Baker	3 copies

DSTO Library

Library Fishermans Bend	1 copy
Library Maribyrnong	1 copy

Library Salisbury	2 copies
Australian Archives	1 copy
Library, MOD, Pyrmont	Doc Data sheet only

Capability Development Division

Director General Maritime Development	Doc Data Sheet only
Director General Land Development	Doc Data Sheet only
Director General C3I Development	Doc Data Sheet only
Director General Aerospace Development	Doc Data Sheet only

Navy

SO (Science), Director of Naval Warfare Maritime Headquarters Annex, Garden Island, NSW 2000.	Doc Data Sheet only
Director of Oceanography and Meteorology Maritime Headquarters Annex, Garden Island, NSW 2000.	1 copy

Army

ABCA Standardisation Officer, Puckapunyal	4 copies
SO (Science), DJFHQ(L), MILPO Enoggera, Queensland 4051	Doc Data Sheet only
NAPOC QWG Engineer NBCD c/- DENGRS-A, HQ Engineer Centre Liverpool Military Area, NSW 2174	Doc Data Sheet only

Intelligence Program

DGSTA Defence Intelligence Organisation	Doc Data Sheet only

Corporate Support Program (libraries)

OIC TRS, Defence Regional Library, Canberra	1 copy
*US Defence Technical Information Center	2 copies
*UK Defence Research Information Centre	2 copies
*Canada Defence Scientific Information Service	1 copy
*NZ Defence Information Centre	1 copy
National Library of Australia	1 copy

UNIVERSITIES AND COLLEGES

Australian Defence Force Academy Library	1 copy
Head of Aerospace and Mechanical Engineering	1 copy
Deakin University, Serials Section (M list), Deakin University Library, Geelong, 3217	1 copy
Senior Librarian, Hargrave Library, Monash University	1 copy
Librarian, Flinders University	1 copy

OTHER ORGANISATIONS

NASA (Canberra)	1 copy
AGPS	1 copy
State Library of South Australia	

Parliamentary Library, South Australia	1 copy

OUTSIDE AUSTRALIA

ABSTRACTING AND INFORMATION ORGANISATIONS

INSPEC: Acquisitions Section Institution of Electrical Engineers	1 copy
Library, Chemical Abstracts Reference Service	1 copy
Engineering Societies Library, US	1 copy
Materials Information, Cambridge Scientific Abstracts, US	1 copy
Documents Librarian, The Center for Research Libraries, US	1 copy

INFORMATION EXCHANGE AGREEMENT PARTNERS

Acquisitions Unit, Science Reference and Information Service, UK	1 copy
Library - Exchange Desk, National Institute of Standards and Technology, US	1 copy
SPARES	6 copies

Total number of copies: **62**

DEFENCE SCIENCE AND TECHNOLOGY ORGANISATION
DOCUMENT CONTROL DATA

1. PRIVACY MARKING/CAVEAT (OF DOCUMENT)

2. TITLE

Refractivity Profile Assimilation Model for the Atmospheric Boundary Layer

3. SECURITY CLASSIFICATION (FOR UNCLASSIFIED REPORTS THAT ARE LIMITED RELEASE USE (L) NEXT TO DOCUMENT CLASSIFICATION)

Document	(U)
Title	(U)
Abstract	(U)

4. AUTHOR(S)

D. M. Phillips and C. P. Baker

5. CORPORATE AUTHOR

Electronics and Surveillance Research Laboratory
PO Box 1500
Salisbury SA 5108 Australia

6a. DSTO NUMBER	6b. AR NUMBER	6c. TYPE OF REPORT	7. DOCUMENT DATE
DSTO-RR-0148	AR-010-884	Research Report	July 1999

8. FILE NUMBER	9. TASK NUMBER	10. TASK SPONSOR	11. NO. OF PAGES	12. NO. OF REFERENCES
B9505/17/63	DST 98/138	DSTO	30	31

13. DOWNGRADING/DELIMITING INSTRUCTIONS

14. RELEASE AUTHORITY

Chief, Surveillance Systems Division

15. SECONDARY RELEASE STATEMENT OF THIS DOCUMENT

Approved for public release

OVERSEAS ENQUIRIES OUTSIDE STATED LIMITATIONS SHOULD BE REFERRED THROUGH DOCUMENT EXCHANGE CENTRE, DIS NETWORK OFFICE, DEPT OF DEFENCE, CAMPBELL PARK OFFICES, CANBERRA ACT 2600

16. DELIBERATE ANNOUNCEMENT

No Limitations

17. CASUAL ANNOUNCEMENT Yes

18. DEFTEST DESCRIPTORS

Atmospheric prediction; Atmospheric boundary layer; Atmospheric refraction; Performance prediction

19. ABSTRACT

Anomalous propagation of microwave radiation in the Atmospheric Boundary Layer (ABL) at near horizontal elevation angles due to small vertical gradients in the refractive index of the air can significantly enhance or degrade the performance of microwave systems. The modelling of microwave propagation under anomalous ducting conditions requires an accurate knowledge of the vertical profile of atmospheric refractivity, which can be derived from profiles of pressure, temperature and moisture. This paper develops the Monin-Obukhov similarity theory of the atmospheric surface layer by blending it into the mixed layer, which lies above it and which forms the bulk of the atmospheric boundary layer. This approach enables the optimal assimilation of meteorological data from a variety of heights in the ABL and a sensitivity analysis provides the necessary weight functions. Application of the theory to one set of data over sea shows that a significant improvement in the fit to the data is achieved when the roughness length for heat is assumed to be much greater than the roughness length for wind.